Hearing Research 333 (2016) 66–76

Contents lists available at ScienceDirect

Hearing Research

journal homepage: www.elsevier.com/locate/heares

Research paper

Selective processing of auditory evoked responses with iterative-randomized stimulation and averaging: A strategy for evaluating the time-invariant assumption

Joaquin T. Valderrama [a, *], Angel de la Torre [b], Carlos Medina [b], Jose C. Segura [b], A. Roger D. Thornton [c]

[a] National Acoustic Laboratories, Australian Hearing Hub, 16 University Avenue, Macquarie University, NSW 2109, Sydney, Australia
[b] Department of Signal Theory, Telematics and Communications, CITIC-UGR, University of Granada, C/ Periodista Daniel Saucedo Aranda s/n, Granada 18071, Spain
[c] MRC Institute of Hearing Research, Royal South Hants Hospital, Southampton SO14 OYG, United Kingdom

ARTICLE INFO

Article history:
Received 21 September 2015
Received in revised form
21 November 2015
Accepted 2 December 2015
Available online 8 January 2016

Keywords:
Randomized stimulation and averaging (RSA)
Jitter
Deconvolution
Evoked potentials
Time-invariant
ABR
MLR
SOA

ABSTRACT

The recording of auditory evoked potentials (AEPs) at fast rates allows the study of neural adaptation, improves accuracy in estimating hearing threshold and may help diagnosing certain pathologies. Stimulation sequences used to record AEPs at fast rates require to be designed with a certain jitter, i.e., not periodical. Some authors believe that stimuli from wide-jittered sequences may evoke auditory responses of different morphology, and therefore, the time-invariant assumption would not be accomplished. This paper describes a methodology that can be used to analyze the time-invariant assumption in jittered stimulation sequences. The proposed method [Split-IRSA] is based on an extended version of the iterative randomized stimulation and averaging (IRSA) technique, including selective processing of sweeps according to a predefined criterion. The fundamentals, the mathematical basis and relevant implementation guidelines of this technique are presented in this paper. The results of this study show that Split-IRSA presents an adequate performance and that both fast and slow mechanisms of adaptation influence the evoked-response morphology, thus both mechanisms should be considered when time-invariance is assumed. The significance of these findings is discussed.

1. Introduction

The conventional auditory evoked potential (AEP) recording method consists in the periodical presentation of stimuli and the average of their associated auditory neural responses (sweeps) in order to increase the signal-to-noise ratio (SNR) (Thornton, 2007). The conventional method presents the limitation that the period of stimulation (i.e., the inverse of the stimulation rate) must be greater than the averaging window, avoiding sweeps to be overlapped (Wong and Bickford, 1980); otherwise it would not be mathematically possible to recover the transient evoked response (Kjaer, 1980). This rate limitation implies that auditory brainstem responses (ABR) and middle latency responses (MLR) cannot be recorded with the conventional technique at rates faster than 100 Hz and 10 Hz, respectively, considering standard averaging windows of 10 ms in ABR and 100 ms in MLR signals. However, the recording of these signals at higher rates present several advantages, such as the study of neural adaptation (Burkard et al., 1990; Lasky, 1997), the diagnosis of certain pathologies (Jiang et al., 2000; Yagi and Kaga, 1979) and better performance in hearing threshold estimation (Leung et al., 1998).

The maximum length sequence (MLS) technique was developed by Eysholdt and Schreiner (1982) to overcome the rate limitation imposed by the conventional technique. This technique was extensively used not only to record AEPs at fast stimulation rates, when the responses are overlapped (Burkard and Palmer, 1997; Eggermont, 1993; Lasky et al., 1995), but also to analyze the linear and non-linear interaction components of otoacoustic emissions (de Boer et al., 2007; Hine et al., 1997, 2001; Lineton et al., 2006).

* Corresponding author.
E-mail addresses: joaquin.valderrama@nal.gov.au (J.T. Valderrama), atv@ugr.es (A. de la Torre), cmedina@ugr.es (C. Medina), segura@ugr.es (J.C. Segura), ardt@soton.ac.uk (A.R.D. Thornton).

http://dx.doi.org/10.1016/j.heares.2015.12.009
0378-5955/

Stimulus-onset asynchrony (SOA), i.e. the distribution of time intervals between adjacent stimuli, are multiples of a minimum pulse interval in MLS sequences, which leads to stimulation sequences of a large jitter (Burkard et al., 1990; Özdamar et al., 2007). The jitter of a stimulation sequence determines dispersion of the SOA distribution.

Several techniques have emerged to deconvolve overlapped AEPs using narrow-jittered stimulation sequences. Some of the most relevant techniques are quasi-periodic sequence deconvolution (QSD) (Jewett et al., 2004), continuous loop averaging deconvolution (CLAD) (Delgado and Özdamar, 2004; Özdamar and Bohórquez, 2006), and least-squares deconvolution (LSD) (Bardy et al., 2014a). These techniques have been successfully used in several research applications (Bardy et al., 2014b; Bohórquez and Özdamar, 2008; Özdamar et al., 2007). The major limitation of these techniques is that obtaining efficient, narrow-jittered stimulation sequences may require an extensive search, since they must accomplish frequency-domain restrictions to avoid noise amplification in the deconvolution process (Jewett et al., 2004; Özdamar and Bohórquez, 2006).

A recently published paper describes iterative randomized stimulation and averaging (IRSA), which allows AEPs to be recorded at fast rates using narrow-jittered sequences (Valderrama et al., 2014c). This is achieved by the estimate and removal of the interference associated with overlapping responses through iterations in the time-domain, providing better estimates of the response in succeeding iterations. This technique assumes that the AEP morphology is time-invariant, i.e., all stimuli evoke the same neural response, which may constrain the flexibility of this technique in certain applications.

Despite the great effort in developing different methodologies to record AEPs at fast rates using narrow-jittered sequences, it is still controversial whether or not stimulation sequences of a wide jitter are a problem. Some authors believe that stimuli in high-jittered sequences may evoke auditory responses of different morphology as a consequence of the effects of neural adaptation, contradicting therefore the time-invariant assumption (Jewett et al., 2004; Özdamar and Bohórquez, 2006; Valderrama et al., 2014b). However, to the best of our knowledge, we have not found any technique that allows evaluation of the time-invariant assumption.

This paper describes an extended version of IRSA [Split-IRSA] which allows selective averaging and processing when AEPs of different morphology are recorded. In this study, the performance of this technique is assessed with both artificially synthesized and real experiments. The Split-IRSA technique is applied to evaluate the time-invariant assumption on ABR and MLR signals recorded with 16 ms-jittered stimulation sequences. The results of this study show that (a) the Split-IRSA technique presents an adequate performance, (b) the time-invariant assumption in auditory responses recorded on jittered stimulation sequences can be evaluated following a methodology based on Split-IRSA, and (c) the morphology of individual sweeps in ABR and MLR signals is influenced by both fast and slow mechanisms of adaptation. The potential of this method and the significance of the findings obtained in this study are discussed.

2. Methods

This section presents the basis and the mathematical formulation of the Split-IRSA technique, the protocols followed in the recording of real electroencephalograms (EEGs), and the objectives, hypotheses and procedures of the experiments.

2.1. Split-IRSA

The fundamentals for the Split-IRSA algorithm are very similar to those of IRSA, described in detail in Valderrama et al. (2014c). AEPs are estimated in Split-IRSA through an iterative process in the time domain. Each iteration includes estimation of the interference associated with overlapping responses, subtraction of this interference from the recorded EEG, and re-estimation of the AEPs. Better AEPs estimates can be obtained recursively since improved AEPs estimates lead to a better interference estimate, which leads to more accurate AEPs estimates. The precision of the AEPs estimates increases with the number of iterations. In contrast to IRSA, this updated formulation [Split-IRSA] allows selective processing of sweeps, and therefore, AEPs of different morphology can be separately estimated.

Stimulation sequences are generated in Split-IRSA as the combination of independent sub-sequences, each of them based on randomized stimulation, in which the SOA of the stimuli vary randomly according to a predefined probability distribution (Valderrama et al., 2012). The Split-IRSA technique retrieves the time-invariant component of the AEPs belonging to each sub-sequence, i.e., it is assumed that all stimuli from the same sub-sequence evoke the same AEP.

The mathematical formulation for the Split-IRSA technique is outlined below. Let $[\boldsymbol{s}_1(n), \boldsymbol{s}_2(n), \ldots, \boldsymbol{s}_T(n)]$ $(n = 1,\ldots,N)$ be T sub-sequences, each of them composed of $[K_1, K_2, \ldots, K_T]$ stimuli that evoke, respectively, T AEPs of different morphology, represented by $[\boldsymbol{x}_1(j), \boldsymbol{x}_2(j), \ldots, \boldsymbol{x}_T(j)]$ $(j = 1,\ldots,J)$, where N and J represent, respectively, the length in samples of the EEG and the averaging window. The recorded EEG $\boldsymbol{y}(n)$, can be modeled as the summation of the convolutions $(*)$ of each sub-sequence with their corresponding AEP plus noise:

$$\boldsymbol{y}(n) = \boldsymbol{s}_1(n)*\boldsymbol{x}_1 + \boldsymbol{s}_2(n)*\boldsymbol{x}_2 + \ldots + \boldsymbol{s}_T(n)*\boldsymbol{x}_T + noise. \quad (1)$$

The AEPs corresponding to each sub-sequence $(\tau = 1,\ldots,T)$ in the iteration i, $\widehat{\boldsymbol{x}}_{\tau,i}(j = 1,\ldots,J)$, are estimated in Split-IRSA according to

$$\widehat{\boldsymbol{x}}_{\tau,i}(j) = \frac{1}{K_\tau}\cdot\sum_{k=1}^{K_\tau}\boldsymbol{y}_{\tau,k}(j + \boldsymbol{m}_\tau(k)), \quad (2)$$

where $\boldsymbol{y}_{\tau,k}$ represents the EEG in which the auditory responses adjacent to the stimulus k (from the sub-sequence τ) are suppressed; and $\boldsymbol{m}_\tau$ is a trigger vector that includes the samples of the EEG in which the stimuli of the sub-sequence τ occur $(k = 1,\ldots,K_\tau)$. The $\boldsymbol{y}_{\tau,k}$ signals can be obtained for each stimulus k at each sub-sequence τ by suppressing from the recorded EEG the AEPs estimated on the preceding iteration $(i-1)$ corresponding to all sub-sequences $(t = 1,\ldots,T)$ and by adding the AEP corresponding to the stimulus k of the sub-sequence τ:

$$\boldsymbol{y}_{\tau,k}(n) = \boldsymbol{y}(n) - \sum_{t=1}^{T}\left[\boldsymbol{s}_t(n)*\widehat{\boldsymbol{x}}_{t,i-1}\right] + \boldsymbol{s}_{\tau,k}(n)*\widehat{\boldsymbol{x}}_{\tau,i-1}, \quad (3)$$

where $\boldsymbol{s}_{\tau,k}$ represents the stimulation sequence for the stimulus k of the sub-sequence τ. Considering $\boldsymbol{z}_i(n)$ as the EEG on the iteration i with all AEPs estimated on the preceding iteration suppressed: $\boldsymbol{z}_i(n) = \boldsymbol{y}(n) - \sum_{t=1}^{T}[\boldsymbol{s}_t(n)*\widehat{\boldsymbol{x}}_{t,i-1}]$, then equation (3) can be rewritten as

$$\boldsymbol{y}_{\tau,k}(n) = \boldsymbol{z}_i(n) + \boldsymbol{s}_{\tau,k}(n)*\widehat{\boldsymbol{x}}_{\tau,i-1}. \quad (4)$$

Hence, the sections of $\boldsymbol{y}_{\tau,k}$ corresponding to the averaging window can be obtained as

$$\boldsymbol{y}_{\tau,k}(j + \boldsymbol{m}_\tau(k)) = \boldsymbol{z}_i(j + \boldsymbol{m}_\tau(k)) + \boldsymbol{s}_{\tau,k}(j + \boldsymbol{m}_\tau(k))*\widehat{\boldsymbol{x}}_{\tau,i-1}. \quad (5)$$

The $\boldsymbol{s}_{\tau,k}(n)$ signal can be expressed as $\boldsymbol{\delta}(n-\boldsymbol{m}_\tau(k))$, where $\boldsymbol{\delta}(n)$

represents the Dirac delta function, with the value 1 for $n = 0$, and 0 otherwise. Since $\boldsymbol{\delta}(n)*\boldsymbol{f}=\boldsymbol{f}$, for whatever function $\boldsymbol{f}$, equation (5) can be expressed as

$$\begin{aligned}\boldsymbol{y}_{\boldsymbol{\tau},\boldsymbol{k}}(j+\boldsymbol{m}_{\boldsymbol{\tau}}(k)) &= \boldsymbol{z}_{\boldsymbol{i}}(j+\boldsymbol{m}_{\boldsymbol{\tau}}(k)) + \boldsymbol{\delta}(n-\boldsymbol{m}_{\boldsymbol{\tau}}(k)+\boldsymbol{m}_{\boldsymbol{\tau}}(k))*\widehat{\boldsymbol{x}}_{\boldsymbol{\tau},\boldsymbol{i}-1} \\ &= \boldsymbol{z}_{\boldsymbol{i}}(j+\boldsymbol{m}_{\boldsymbol{\tau}}(k)) + \widehat{\boldsymbol{x}}_{\boldsymbol{\tau},\boldsymbol{i}-1}.\end{aligned} \tag{6}$$

Therefore, from equation (2), the AEP estimate on the iteration i can be obtained as

$$\begin{aligned}\widehat{\boldsymbol{x}}_{\boldsymbol{\tau},\boldsymbol{i}}(j) &= \frac{1}{K_{\tau}}\cdot\sum_{k=1}^{K_{\tau}}\left[\boldsymbol{z}_{\boldsymbol{i}}(j+\boldsymbol{m}_{\boldsymbol{\tau}}(k)) + \widehat{\boldsymbol{x}}_{\boldsymbol{\tau},\boldsymbol{i}-1}\right] \\ &= \widehat{\boldsymbol{x}}_{\boldsymbol{\tau},\boldsymbol{i}-1} + \frac{1}{K_{\tau}}\cdot\sum_{k=1}^{K_{\tau}}\boldsymbol{z}_{\boldsymbol{i}}(j+\boldsymbol{m}_{\boldsymbol{\tau}}(k)).\end{aligned} \tag{7}$$

Similar to IRSA, we have found in simulations and real data that Split-IRSA might present problems of instability, where succeeding iterations lead to worse AEP estimates. Instability might be especially relevant in low-jittered stimulation sequences in which the averaged SOA is significantly lower than the averaging window, e.g., with a high-degree of overlap. Problems of instability can be solved using a correction factor (α) that weights the correction $\frac{1}{K_{\tau}}\cdot\sum_{k=1}^{K_{\tau}}\boldsymbol{z}_{\boldsymbol{i}}(j+\boldsymbol{m}_{\boldsymbol{\tau}}(k))$ made on the preceding AEP estimate. Low α values ensure convergence, but require a greater number of iterations to converge. The greatest α that avoids instability is optimal. Thus, the inclusion of this correction factor onto equation (7) leads to:

$$\widehat{\boldsymbol{x}}_{\boldsymbol{\tau},\boldsymbol{i}}(j) = \widehat{\boldsymbol{x}}_{\boldsymbol{\tau},\boldsymbol{i}-1} + \alpha\cdot\frac{1}{K_{\tau}}\cdot\sum_{k=1}^{K_{\tau}}\boldsymbol{z}_{\boldsymbol{i}}(j+\boldsymbol{m}_{\boldsymbol{\tau}}(k)). \tag{8}$$

The number of iterations can be defined either as a fixed value I ($\widehat{\boldsymbol{x}}_{\boldsymbol{\tau}} = \widehat{\boldsymbol{x}}_{\boldsymbol{\tau},\boldsymbol{I}}\,\forall\,\tau$) or automatically considering whether the differences between AEP estimates in succeeding iterations are negligible ($\widehat{\boldsymbol{x}}_{\boldsymbol{\tau}} = \widehat{\boldsymbol{x}}_{\boldsymbol{\tau},\boldsymbol{i}} \Leftrightarrow \widehat{\boldsymbol{x}}_{\boldsymbol{\tau},\boldsymbol{i}} \approx \widehat{\boldsymbol{x}}_{\boldsymbol{\tau},\boldsymbol{i}-1}\,\forall\,\tau$).

Fig. 1 illustrates an example of the performance of the Split-IRSA technique under a simulation framework. In this example, a stimulation sequence $\boldsymbol{s}(n)$ was generated containing 4000 stimuli in which the SOA varied randomly between 20 and 30 ms [short SOA sub-sequence: $\boldsymbol{s}_1(n)$] and between 60 and 70 ms [long SOA sub-sequence: $\boldsymbol{s}_2(n)$]. Fig. 1A shows the histogram of the SOA of this stimulation sequence, where the sub-sequences $\boldsymbol{s}_1(n)$ and $\boldsymbol{s}_2(n)$ can be identified. Fig. 1B shows the configuration settings of this simulation experiment. Fig. 1B1 shows a frame of the first 20.000 samples of $\boldsymbol{s}(n)$, using a sampling frequency of 25 kHz. In this segment, long- and short-SOA stimuli can be visually identified. Fig. 1B2 and B3 show, respectively, the triggers corresponding to each sub-sequence. In these sub-sequences, the first three elements of the trigger vectors [$\boldsymbol{m}_1$ and $\boldsymbol{m}_2$] are labeled as a reference. An artificially synthesized EEG was generated as the summation of the convolutions of the sub-sequences $\boldsymbol{s}_1(n)$ and $\boldsymbol{s}_2(n)$ with two high-quality real MLR signals of different morphology: $\boldsymbol{x}_1$ and $\boldsymbol{x}_2$. The $\boldsymbol{x}_1$ and $\boldsymbol{x}_2$ signals are shown next to the first stimulus in each sub-sequence. These signals were recorded from two normal hearing subjects (males, 28 and 26 yr, respectively) using 4800 stimuli presented at 70 dB HL at an average rate of 40 Hz and processed by the IRSA technique. The artificially synthesized EEG [$\boldsymbol{y}(n)$], along with the triggers corresponding to both sub-sequences, are shown in Fig. 1B4. In this experiment, passband-filtered noise (Butterworth, 4th order, [30–200] Hz) was added to $\boldsymbol{y}(n)$ at a SNR of −5 dB (Fig. 1B5). Fig. 1C presents the normalized energy of the averaged residual, evaluated as $\frac{1}{N}\sum_{n=1}^{N}\boldsymbol{z}_{\boldsymbol{i}}(n)^2$, at different number of iterations for different α values. This figure shows that the α parameter can be used to control convergence and avoid instability. In this example, α values 1.3 and 1.0 cause instability, where the averaged residual increases in succeeding iterations. In contrast, the averaged residual for α values 0.8 and 0.1 decreases with the number of iterations, which means that better estimates of the responses are obtained recursively. This figure shows that although both α values 0.8 and 0.1 tend to converge, the convergence for α value 0.1 requires a larger number of iterations, i.e., it is less efficient. This simulation shows that α equal to 0.8 and 5 iterations are appropriate values to obtain accurate estimates of the signals $\boldsymbol{x}_1$ and $\boldsymbol{x}_2$. Fig. 1D1 and D2 show, respectively, the AEP estimates for $\boldsymbol{x}_1$ and $\boldsymbol{x}_2$ at the second, fifth and tenth iteration for α-value of 1.3. These figures show an example of instability, where worse estimates of the responses are obtained in succeeding iterations, i.e., the root-mean-square (RMS) error between the template and the MLR estimate increases in succeeding iterations. Fig. 1E1 and E2 show, respectively, the first three estimates of the signals $\boldsymbol{x}_1$ and $\boldsymbol{x}_2$ for an α value 0.8. In this example, when the α value is selected appropriately, better estimates are obtained recursively, i.e., the RMS error decreases with increasing iterations [convergence scenario].

A software routine programmed in MATLAB (The Mathworks, Inc., Natick, MA) that implements the Split-IRSA technique is available as supporting information in this paper (Appendix A).

2.2. EEG recording and processing

The EEG recording process consisted in the presentation of stimuli to a subject and the recording of their associated neural response through surface disposable electrodes (Ambu Neuroline 720, Ambu A/S, Denmark) placed on the skin at different positions on the head. The positive electrode was placed at the high-forehead, the negative electrode at the ipsilateral mastoid and the reference electrode at the low-forehead. The interelectrode impedance was below 5 kΩ in all recordings. Stimuli consisted of 100 μs-duration, monophasic clicks delivered in rarefaction polarity at 70 dB HL (corresponding to 103.54 dB peak-to-peak equivalent sound pressure level) through the Etymotic ER-3A insert earphones (Etymotic Research, Inc., Elk Grove Village, IL). Calibration was carried out according to the ISO-389 standard, using an Artificial Ear type 4153 2-cc acoustic coupler (Brüel & Kjær Sound & Vibration Measurements A/S, Nærum, Denmark). The recording sessions took place in the MRC Institute of Hearing Research (Royal South Hants Hospital, Southampton, United Kingdom), in a sound-shielded screening booth prepared to attenuate electrical and electromagnetic interference. Subjects were comfortably seated in order to minimize electromyogenic noise. The signal recorded by the electrodes was 86 dB amplified (gain ×20.000) and bandpass filtered by a 24 dB/Octave slope filter with a bandwidth of [0.5–3500] Hz. The amplified EEG was sampled at 25 kHz and quantized with a resolution of 16 bits. Digitized EEGs were digitally filtered by a 4th order Butterworth filter ([200–2000] Hz for ABR and [30–1500] for MLR). Group delays introduced by the insert earphones (0.81 ms) (Elberling et al., 2012) and by both analog and digital filters were digitally compensated. Data processing was carried out by custom-designed scripts implemented in MATLAB. The features of the AEP recording system used in this study are presented in Valderrama et al. (2014a).

Analysis of AEPs consisted in the measurement of their most relevant components in terms of latencies and amplitudes.

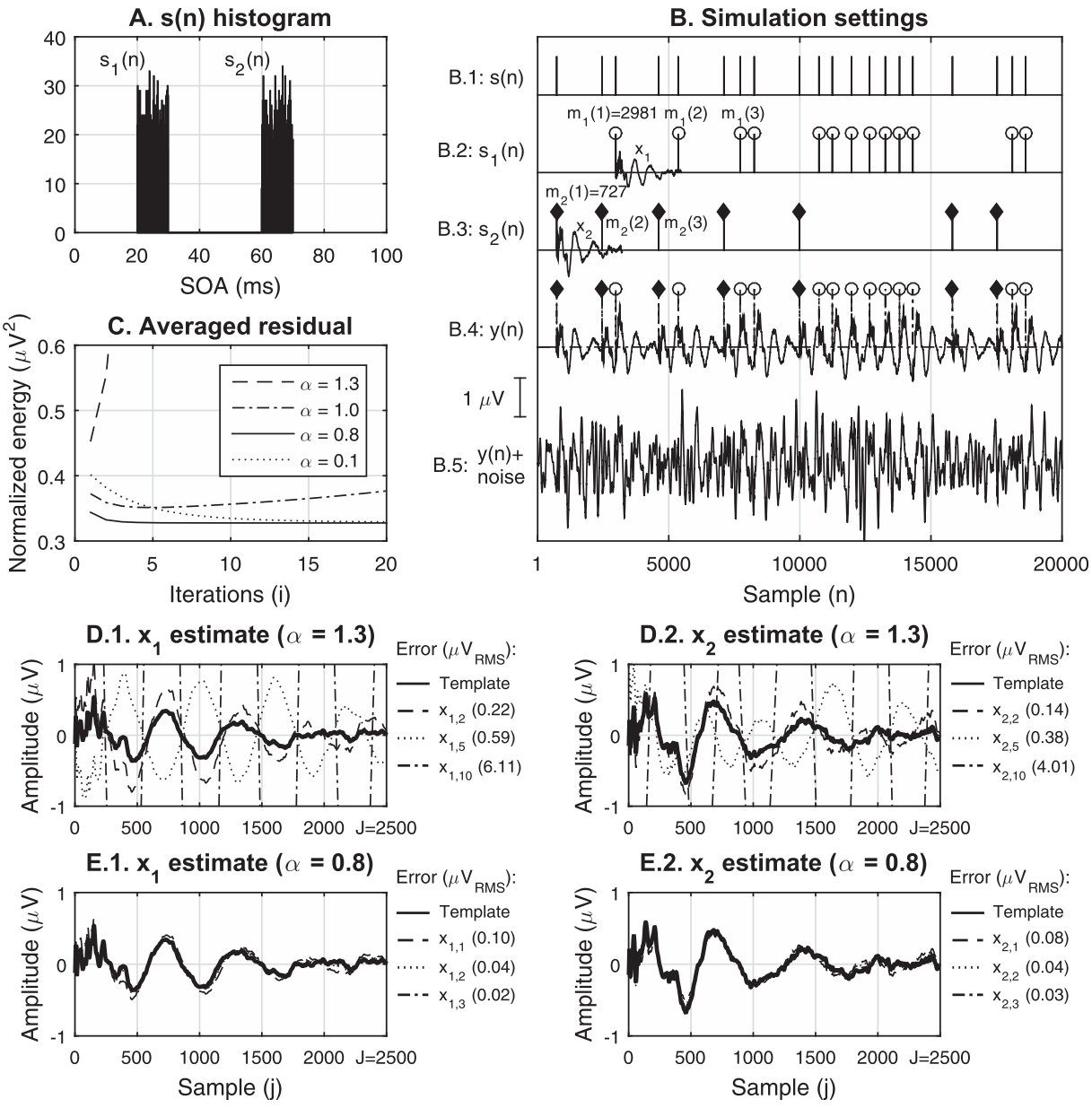

Fig. 1. Performance and parameters involved on the Split-IRSA technique. (A) Histogram of the inter-stimulus interval (SOA) of an example stimulation sequence $\boldsymbol{s}(n)$. The subsequences $\boldsymbol{s}_1(n)$ and $\boldsymbol{s}_2(n)$ are marked on the figure. (B) Parameter settings of this experiment. (C) Normalized energy (μV^2) of the averaged residual, $\frac{1}{K_r}\cdot\sum_{k=1}^{K_r}\boldsymbol{z_i}(j+\boldsymbol{m}_r(k))$, at different iterations and α-values. This figure shows that instability problems (normalized energy increases with the number of iterations) can be avoided by selecting an appropriate value of α. (D.1 and D.2) Evoked potential estimates at different iterations under instability: worse estimates are obtained in succeeding iterations. (E.1 and E.2) Evoked potential estimates at different iterations in a convergence scenario: better estimates are obtained in succeeding iterations, e.g., error between the original template and the estimates decrease as iterations increase.

Latencies were measured as the time difference in milliseconds from stimulus onset to the occurrence of the components. Amplitudes were estimated in ABR as the difference in microvolts between the top of the peak and the following trough, whereas in MLR, amplitudes were measured as the difference between the positive and negative peaks of the wave complex (Burkard and Don, 2007).

The recording protocols followed in the experiments of this work were in accordance with the Code of Ethics of the World Medical Association (Declaration of Helsinki) for experiments involving humans, and were approved by the Research Ethics Committee established by the Health Research Authority (Reference No. RHM ENT0082).

2.3. Description of the experiments

2.3.1. Rationale

Three experiments were carried out with the double purpose of evaluating the performance of the Split-IRSA technique and the validity of the time-invariant assumption in the recording of ABR and MLR signals with 16 ms-jittered randomized stimulation sequences.

2.3.2. Subjects

All subjects tested on the experiments of this study were volunteers, reported no history of auditory dysfunction and presented normal hearing sensitivity at octave frequencies ([250–8000] Hz).

These subjects were paid and gave written consent to participate.

2.3.3. Experiment 1

The first experiment compares ABR and MLR real signals recorded on one subject (male, 30 yr) at different rates in two scenarios.

In scenario 1, ABR signals were recorded at 16 different rates using 1 ms-jittered sequences: $SOA_{15\text{-}16}$ (65 Hz), $SOA_{14\text{-}15}$ (69 Hz), $SOA_{13\text{-}14}$ (74 Hz), $SOA_{12\text{-}13}$ (80 Hz), $SOA_{11\text{-}12}$ (87 Hz), $SOA_{10\text{-}11}$ (95 Hz), $SOA_{9\text{-}10}$ (105 Hz), $SOA_{8\text{-}9}$ (118 Hz), $SOA_{7\text{-}8}$ (133 Hz), $SOA_{6\text{-}7}$ (154 Hz), $SOA_{5\text{-}6}$ (182 Hz), $SOA_{4\text{-}5}$ (222 Hz), $SOA_{3\text{-}4}$ (286 Hz), $SOA_{2\text{-}3}$ (400 Hz), $SOA_{1\text{-}2}$ (667 Hz), $SOA_{0\text{-}1}$ (2000 Hz); and MLR signals were recorded at 4 different rates using 4 ms-jittered sequences: $SOA_{12\text{-}16}$ (71 Hz), $SOA_{8\text{-}12}$ (100 Hz), $SOA_{4\text{-}8}$ (167 Hz) and $SOA_{0\text{-}4}$ (500 Hz). A large number of stimuli were used in each stimulation sequence in order to obtain signals of sufficient quality. In ABR signals, sequences $SOA_{15\text{-}16}$ to $SOA_{9\text{-}10}$ included 12,500 stimuli, while sequences $SOA_{8\text{-}9}$ to $SOA_{0\text{-}1}$ contained 20,000 stimuli. The larger number of stimuli in higher-rate sequences was used to accommodate the loss of SNR due to the reduction of amplitude of the components as a consequence of adaptation (Hine et al., 2001). In MLR signals, all sequences contained 50.000 stimuli. ABR and MLR signals on this scenario were processed by the IRSA technique (Valderrama et al., 2014c). The number of iterations for ABR and MLR signals were, respectively 50 and 500. The value of α was 0.8 at all rates for ABR signals, except for the sequences $SOA_{5\text{-}6}$, $SOA_{4\text{-}5}$, $SOA_{3\text{-}4}$ and $SOA_{2\text{-}3}$, where α was 0.5. In MLR signals, the α-value for $SOA_{12\text{-}16}$ and $SOA_{8\text{-}12}$ was 0.3; for $SOA_{4\text{-}8}$, α was 0.5; and for $SOA_{0\text{-}4}$, α was 0.8. We tested in simulations that these parameters were appropriate to obtain accurate ABR and MLR estimates.

In scenario 2, ABR and MLR signals were estimated on the same subject and at the same stimulation rates as for scenario 1 from a single EEG corresponding to a stimulation sequence $SOA_{0\text{-}16}$ (jitter of 16 ms) of 200,000 stimuli. In ABR, each stimulus was categorized in 1 ms-jittered sub-sequences according to their preceding stimulus: $\boldsymbol{s}_1$ ($SOA_{0\text{-}1}$: preceding SOA belongs to the interval [0-1]), $\boldsymbol{s}_2$ ($SOA_{1\text{-}2}$), $\boldsymbol{s}_3$ ($SOA_{2\text{-}3}$), …, $\boldsymbol{s}_{16}$ ($SOA_{15\text{-}16}$). Equally, the processing of MLR signals included the categorization of the stimuli according to the intervals: $\boldsymbol{s}_1$ ($SOA_{0\text{-}4}$: preceding SOA belongs to the interval [0-4]), $\boldsymbol{s}_2$ ($SOA_{4\text{-}8}$), $\boldsymbol{s}_3$ ($SOA_{8\text{-}12}$) and $\boldsymbol{s}_4$ ($SOA_{12\text{-}16}$). Since randomized stimulation sequences used in this experiment were distributed according to uniform distributions, the number of stimuli that belonged to each sub-sequence was approximately 12,500 in ABR signals (200,000/16), and 50,000 stimuli in MLR signals (200,000/4). ABR and MLR signals were processed with Split-IRSA, as described in section 2.1 of this paper. The number of iterations (I) and the α-value were, respectively, $I = 50$ and $\alpha = 0.8$ in ABR; and $I = 500$ and $\alpha = 0.8$ in MLR. Experiments in simulations validated the value of these parameters.

The morphology of the ABR and MLR signals obtained in both described scenarios was compared in terms of amplitudes and latencies. The morphology of the auditory responses obtained at different rates on the two scenarios is expected to be influenced by both fast and slow mechanisms of adaptation. On the one hand, the morphology of ABR and MLR signals obtained on scenario 1 is expected to be in accordance with several previous studies in which ABR and MLR signals are recorded at fast rates (Lasky, 1997; Özdamar et al., 2007; Yagi and Kaga, 1979). On the other hand, there is not sufficient literature to hypothesize the ABR and MLR waveforms on scenario 2. If fast mechanisms of adaptation (with a time-constant of a few milliseconds) prevail over slow mechanisms (with a time-constant of several tens of milliseconds), the morphology of the AEPs in scenario 2 will be similar to those in scenario 1, since the morphology of the responses would be strongly influenced by the preceding SOA. In contrast, if slow mechanisms of adaptation prevail over fast mechanisms, then the AEPs corresponding to different sub-sequences would be similar, since the morphology of the response to each stimulus would not be very much influenced by its preceding SOA, but by the averaged SOA of several milliseconds in advanced.

2.3.4. Experiment 2

The objective of experiment 2 is to analyze the performance of the Split-IRSA technique in order to validate the experimental results obtained in experiment 1. This analysis was carried out through a simulation, in which the acquisition settings of experiment 1 were reproduced. This study was performed for ABR and MLR signals, both with and without added noise.

First, a $SOA_{0\text{-}16}$ randomized stimulation sequence of 200.000 stimuli was generated. Each stimulus from this sequence was categorized into sub-sequences as described in scenario 2 in experiment 1, i.e., in the study with ABR signals there were 16 sub-sequences of 1 ms jitter: $\boldsymbol{s}_1$ ($SOA_{0\text{-}1}$), $\boldsymbol{s}_2$ ($SOA_{1\text{-}2}$), …, $\boldsymbol{s}_{16}$ ($SOA_{15\text{-}16}$); and in the study with MLR signals, there were 4 sub-sequences of 4 ms jitter: $\boldsymbol{s}_1$ ($SOA_{0\text{-}4}$), $\boldsymbol{s}_2$ ($SOA_{4\text{-}8}$), …, $\boldsymbol{s}_4$ ($SOA_{12\text{-}16}$). Second, two artificially synthesized EEGs (one for each scenario) were built as the convolution of the stimuli belonging to each sub-sequence with the corresponding ABR/MLR signals obtained in experiment 1 on scenarios 1 and 2. These artificially synthesized EEGs represent the overlapping evoked potentials without any type of noise or artifacts. Finally, the ABR/MLR signals corresponding to each sub-sequence were estimated from these synthesized EEGs using the Split-IRSA technique at the iterations $I = [0, 10, 20, 50]$ in ABR, and $I = [0, 10, 20, 50, 100, 200, 500]$ in MLR. The α-value used in these simulations was the same as in experiment 1, i.e., $\alpha = 0.8$ in both ABR and MLR signals. The error between the original ABR/MLR signals (templates) and the estimated signals was calculated in terms of RMS value.

The same study was repeated including filtered noise (4th order Butterworth, [200–2000] Hz for ABR and [30–1500] for MLR) added to the synthesized EEGs at a RMS value similar to the recorded real EEG. This RMS value was estimated on the recorded EEG after digital filtering (4th order Butterworth, [200–2000] Hz for ABR and [30–1500] for MLR). The estimated RMS values were 1.7 μV for ABR and 3.5 μV for MLR. In ABR signals, the SNRs on the noisy EEGs were −29.2 dB in scenario 1 and -30.2 dB in scenario 2. In MLR, the SNR-values were −17.8 dB in scenario 1 and −23.4 dB in scenario 2.

2.3.5. Experiment 3

In this experiment, we analyzed the morphology of ABR and MLR signals evoked by stimuli that belong to different rate-subsets from stimulation sequences of 16 ms-jitter in order to evaluate the time-invariant assumption.

8 subjects (5 males, 27 ± 4 yr) participated in this study. Each subject was presented a randomized stimulation sequence $SOA_{0\text{-}16}$ of 60.000 stimuli. A single EEG was recorded from each subject. These EEGs were digitally filtered (4th order Butterworth) using a bandwidth [200–2000] Hz for the ABR analysis and [30–1500] Hz for MLR. Sub-sequences were defined as described in scenario 2 on experiment 1 of this paper: $\boldsymbol{s}_1$ ($SOA_{0\text{-}1}$), $\boldsymbol{s}_2$ ($SOA_{1\text{-}2}$), …, $\boldsymbol{s}_{16}$ ($SOA_{15\text{-}16}$) in ABR; and $\boldsymbol{s}_1$ ($SOA_{0\text{-}4}$), $\boldsymbol{s}_2$ ($SOA_{4\text{-}8}$), …, $\boldsymbol{s}_4$ ($SOA_{12\text{-}16}$) in MLR. ABR and MLR signals were estimated from each rate-subset using the Split-IRSA technique, as described in section 2.1 of this paper, using $\alpha = 0.8$, $I = 50$ in ABR and $I = 500$ in MLR. In addition, we used as reference the ABR/MLR signal obtained from the complete stimulation sequence, assuming that all stimuli from the sequence evoked the same response. These signals were obtained using the

IRSA technique ($\alpha = 0.8$, $I = 50$ in ABR and $I = 500$ in MLR) (Valderrama et al., 2014c).

The latencies and amplitudes of waves III and V were measured on ABR signals. In MLR, we measured the latencies for the Na, Pa, Nb and Pb components and the amplitudes for the Na–Pa, Pa–Nb and Nb–Pb wave-complexes. The influence of the average rate in each sub-sequence on the morphology of ABR/MLR signals was evaluated through linear correlation hypothesis tests, considering the slope equal to zero as the null hypothesis of the tests.

The inter-subject variability of the fast adaptation was analyzed in each subject for each parameter as the difference of latencies and ratio of amplitudes between the averaged values corresponding to the intervals [1–8] ms and [8–16] ms, i.e. $L_{[1\text{-}8]}$-$L_{[8\text{-}16]}$ and $A_{[1\text{-}8]}/A_{[8\text{-}16]}$, both in ABR and MLR signals. These parameters evaluate the changes on the waveform morphology depending solely on the previous SOA, thus directly associated with the fast adaptation. The Pb component was excluded from this analysis because of insufficient clear measures of this component, especially at high rates.

3. Results

3.1. Experiment 1

Fig. 2 shows a comparison of the morphology of ABR and MLR signals obtained from one subject at different rates in two different recording-scenarios. The ABR signals used in this study, along with an analysis of the latency and amplitude of the wave V component, are presented in Fig. 2A1, A2 and A3 respectively. Comparison of the morphology of ABR signals in both scenarios show remarkable differences. In scenario 1, as rate increases, the latency of the ABR components increases and the amplitude decreases, which is consistent with several previous studies (Jiang et al., 2009; Stone et al., 2009). However in scenario 2, the latency of wave V seems to be unaltered by rate, and the slope of the linear regression curve of the wave V amplitude obtained at each SOA range is lower than in scenario 1, which suggests that as rate increases, the amplitude of wave V decreases more slowly. ABR signals of both scenarios obtained at rates faster than 400 Hz ($SOA_{2\text{-}3}$) showed a high-level of adaptation and no wave V component could be identified.

Fig. 2B1 shows the MLR signals obtained in this study. The Na, Pa, Nb and Pb components are labeled on the $SOA_{8\text{-}12}$ MLR signal on this figure. All components could be identified at all rates, except Nb and Pb at 500 Hz ($SOA_{0\text{-}4}$) in both scenarios. The values of latency and amplitude of the MLR components obtained in scenario 1 are consistent with those reported on previous studies, in which MLR signals were recorded at fast rates (Özdamar et al., 2007). Fig. 2B2 shows the latencies and a linear regression analysis for the Na, Pa, Nb and Pb components at different rates. This analysis shows that, while Na latency is similar in both scenarios, the latency drift in the rest of the components is more accentuated in scenario 1 than in scenario 2. Analysis of amplitudes for the wave complexes Na–Pa, Pa–Nb and Nb–Pb is presented on Fig. 2B3, B4 and B5 respectively. These figures show that, although amplitudes decrease as rate increases in both scenarios, amplitudes in scenario 1 present a greater value and the slope of the linear regression analysis is steeper in scenario 1 than in scenario 2. Data shown in this experiment is obtained from a single subject. A more robust study of amplitudes and latencies is presented in experiment 3 of this paper.

3.2. Experiment 2

Fig. 3 shows the MLR signals used as reference (templates) and the MLR estimates by the Split-IRSA technique at a different number of iterations in a simulation study. Fig. 3A1 and A2 show, respectively, the results of this study when no noise is added to the synthesized EEG in scenarios 1 and 2. These figures show that the accuracy of the MLR estimates increases with the number of iterations. The MLR estimates obtained with 500 iterations in both scenarios approximate accurately the original templates (errors lower than 0.0002 μV_{RMS} in all cases). Fig. 3B1 and B2 show the results of a similar study in which noise was added to the synthesized EEG at a similar RMS value as in a real situation. As in the no-noise case, the accuracy of the MLR estimates increases with the number of iterations. Although the MLR estimates obtained with 500 iterations in panel B present greater error-values than in the case of EEGs without added noise (panel A), these MLR estimates approximate the morphology of the original templates with sufficient accuracy to estimate correctly the amplitudes and latencies of the main components of these signals.

A similar study was carried out with ABR signals. The results of this study are consistent with those obtained in the study with MLR signals. These results indicate the ABR estimated by Split-IRSA after 50 iterations in both scenarios fit perfectly the templates (error

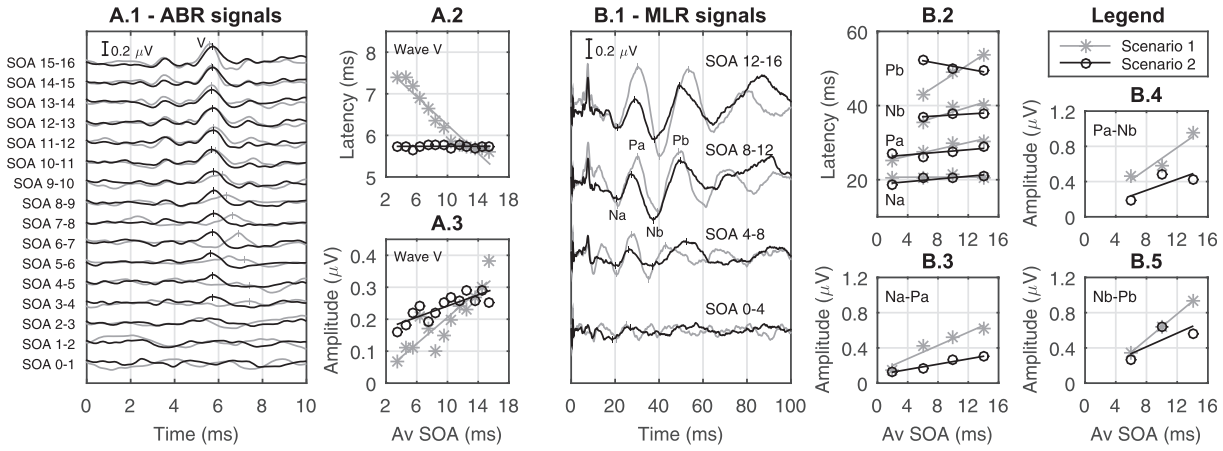

Fig. 2. Comparison of the morphology of ABR and MLR signals recorded from one subject (scenario 1) by narrow-jittered stimulation sequences and processed by IRSA and (scenario 2) by a single 16 ms-jittered stimulation sequence and processed by the Split-IRSA technique in different subsets of stimuli. (A.1) ABR signals obtained at different average SOA (Av SOA) in each scenario. (A.2 and A.3) Latency (ms) and amplitude (μV) of wave V and linear regression analysis evaluated at different rates in scenarios 1 and 2. (B.1) MLR signals obtained in each scenario and rate. (B.2) Latencies (ms) and linear regression analysis measured on the components Na, Pa, Nb and Pb at different rates in each scenario. (B.3, B.4 and B.5) Amplitudes (μV) and linear regression analysis of the waves complexes Na–Pa, Pa–Nb and Nb–Pb at different rates in both scenarios.

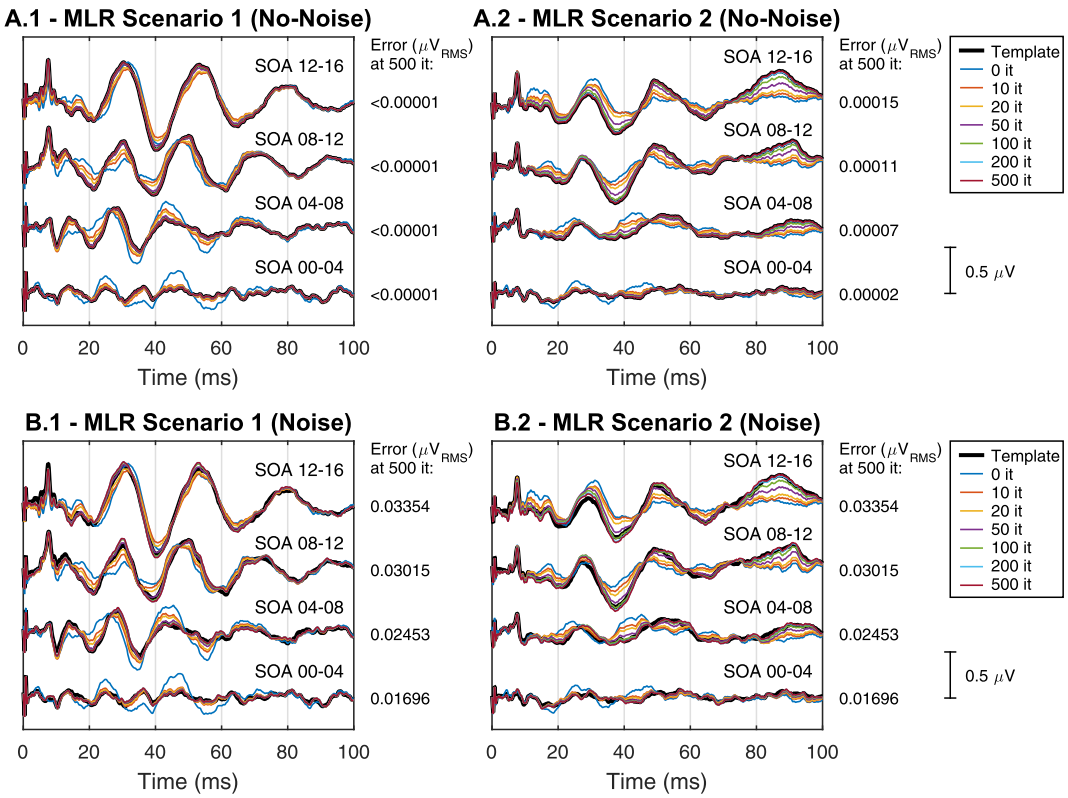

Fig. 3. (Color online) MLR signals estimated by the Split-IRSA technique at a different number of iterations in a simulation study that reproduces the acquisition settings of experiment 1 when no noise is added to the synthesized EEG (panel A) and when noise is added at a similar RMS value as in a real situation (panel B). Errors between the MLR estimates obtained at 500 iterations and the original templates are shown in μV_{RMS}.

estimates <0.00001 μV_{RMS}) when no noise is added to the synthesized EEG. The ABR estimates in both scenarios when noise is added to the EEG present a higher level of noise, but the morphology of these estimates approximates the original templates. The figures that present the morphology of these ABR estimates are available as supplementary material in Appendix B. This appendix also includes tables with the RMS errors between the templates and the ABR/MLR estimates obtained in each scenario at each iteration analyzed in this study.

The results of this experiment point out that (a) the Split-IRSA technique is able to estimate accurately templates of different morphology in different jittering conditions, and (b) the parameters α-value and number of iterations selected on experiment 1 in this paper ($I = 50$ in ABR, $I = 500$ in MLR, $\alpha = 0.8$) are appropriate.

3.3. Experiment 3

Fig. 4 shows the grand-average ABR and MLR waveforms from a set of 8 normal hearing subjects. Subject 2 was not included in the grand-average ABR waveforms since no clear components could be identified. Thick lines in the upper section on each panel represent the ABR and MLR signals obtained directly from the $SOA_{0\text{-}16}$ stimulation sequences, considering that all stimuli evoked the same response (time-invariant assumption). The main components of ABR and MLR are labeled on these signals. The rest of the lines represent the ABR/MLR responses corresponding to different rate-subsets obtained by the Split-IRSA technique, e.g., the ABR waveform corresponding to $SOA_{15\text{-}16}$ is obtained from the auditory responses corresponding to stimuli whose preceding SOA belonged to the interval [15–16] ms. This figure allows an overall study of the morphology of these signals across subjects. This figure shows that the morphology of ABR signals at different rate-subsets is very similar to the signal obtained from the complete stimulation sequence (upper-panel line), except for the ABRs obtained at very fast rates, i.e., $SOA_{2\text{-}3}$ and higher rates, where the latencies of the main components increase and their amplitude decrease significantly. On MLR signals, their morphology vary across different rate-subsets, especially at higher rates. The individual ABR and MLR signals obtained in each subject are available as supplementary material (appendix C).

Fig. 5 and Table 1 show the results of the linear regression analysis of the latencies (L) and amplitudes (A) of the main components of ABR (panel A) and MLR (panel B) signals versus the SOA intervals. The linear regression analyses in panel A show, on one hand, absence of statistically significant evidence for latencies and amplitudes being influenced by rate in the [4–16] ms SOA interval, and on the other, statistically significant evidence of variations on the amplitudes in the [0–8] ms SOA interval. These results point out that the time-invariant assumption is accomplished in ABR along the [4–16] ms SOA interval, but not at the fastest rates. The linear regression analyses in panel B show statistically significant evidence of variations of the morphology of MLR signals at different SOA intervals, thus indicating that the time-invariant assumption is not accomplished.

The inter-subject variability of the fast adaptation is analyzed in Fig. 6. This figure shows a significant variability across subjects. For instance: (a) subjects S1, S7 and S8 show a larger fast adaptation on the latency of ABR wave III than subjects S4, S5 and S6; (b) subject S4 shows a particular low fast adaptation on the amplitude of ABR waves III and V; (c) S4 is also the only subject in which the latency of the ABR wave V and the MLR Na components decreased at high rates; and, (d) subjects S1 and S2 show a lower fast adaptation than

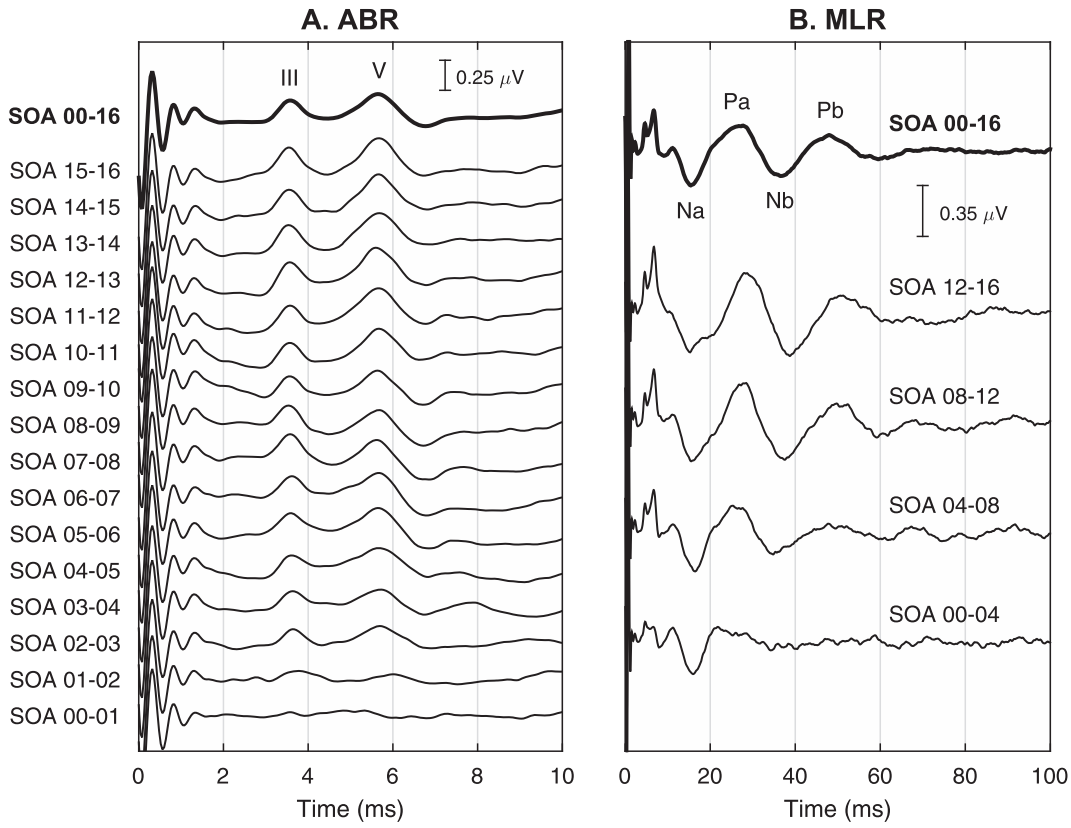

Fig. 4. Grand-average ABR (panel A) and MLR (panel B) waveforms from a set of 8 normal hearing subjects. Thick lines represent the ABR/MLR signals obtained from the complete sequence $SOA_{0\text{-}16}$, and standard lines show the responses obtained at each rate-subset by the Split-IRSA technique.

the rest of the subjects on the latency of the MLR Pa and Nb components. In addition, this study shows a large variability across different parameters within the same subject. For example, subject S1 is the subject showing the largest fast adaptation on the Na latency, but it is also the subject presenting the lowest fast adaptation on the latency of the Pa and Nb components.

4. Discussion

This paper presents a full description of the iterative-randomized stimulation and averaging Split (Split-IRSA) technique. The fundamentals of this technique are similar to IRSA, described in Valderrama et al. (2014c), with the difference that Split-IRSA includes selective processing of responses, i.e., each response can be individually processed and categorized according to a predefined criteria. Split-IRSA allows, therefore, overlapping auditory evoked responses of different morphology to be obtained by an iterative procedure in the time domain. The main advantages of the Split-IRSA technique are: (a) stimulation sequences are based on randomized stimulation, which allows the amount of jitter to be under control; (b) this technique includes a mechanism to control convergence (α-value); (c) Split-IRSA is easy to implement (programming code attached on appendix A of this paper); and (d) it allows selective processing of auditory responses.

The performance of the Split-IRSA technique was validated in this paper through experiments with both simulation and real data. The results of these experiments point out that this technique presents an adequate performance when the α-value and the number of iterations are correctly defined. The simulation study presented in experiment 2 shows that the AEP estimates obtained with Split-IRSA on the first iteration (blue signals on Fig. 3 and in appendix B on this paper) were not accurate, i.e., they present a morphology different from the template signal. This is consistent with results presented in Valderrama et al. (2014c), where we found that interference associated with overlapping responses introduces an artifact in the AEP estimate which cannot be reduced by averaging when the amount of jitter of the stimulation sequence is lower than the dominant period of the recorded AEPs (i.e., 2 ms in ABR and 25 ms in MLR). Thus, a single iteration was not sufficient to obtain accurate AEP estimates. The results of experiment 2 show that more accurate ABR/MLR estimates can be obtained recursively. The results of experiments 1 and 3 in this paper point out that the Split-IRSA technique has allowed real ABR and MLR signals of different morphologies to be recorded simultaneously at very rapid rates using narrow-jittered stimulation sub-sequences.

The flexible nature of Split-IRSA is appropriate for research purposes. In this paper, we have used this technique to analyze the variations in the morphology of ABR and MLR signals across different rate-subsets in 16 ms-jittered stimulation sequences in order to evaluate the time-invariant assumption all along the stimulation sequence. This topic may be of interest as time-invariance is assumed in all techniques that process evoked potentials (Bardy et al., 2014a; Jewett et al., 2004; Özdamar and Bohórquez, 2006), and secondly, it is still not clear whether or not the amount of jitter of a stimulation sequence is a critical parameter to be considered when assuming that each stimulus evokes the same ABR/MLR response (Jewett et al., 2004; Özdamar and Bohórquez, 2006). As far as we are concerned, the methodology presented in this paper is the first attempt to analyze the time-invariant assumption in real ABR and MLR signals obtained in a specific jittered stimulation sequence.

Analysis of ABR and MLR waveforms obtained in scenarios 1 and

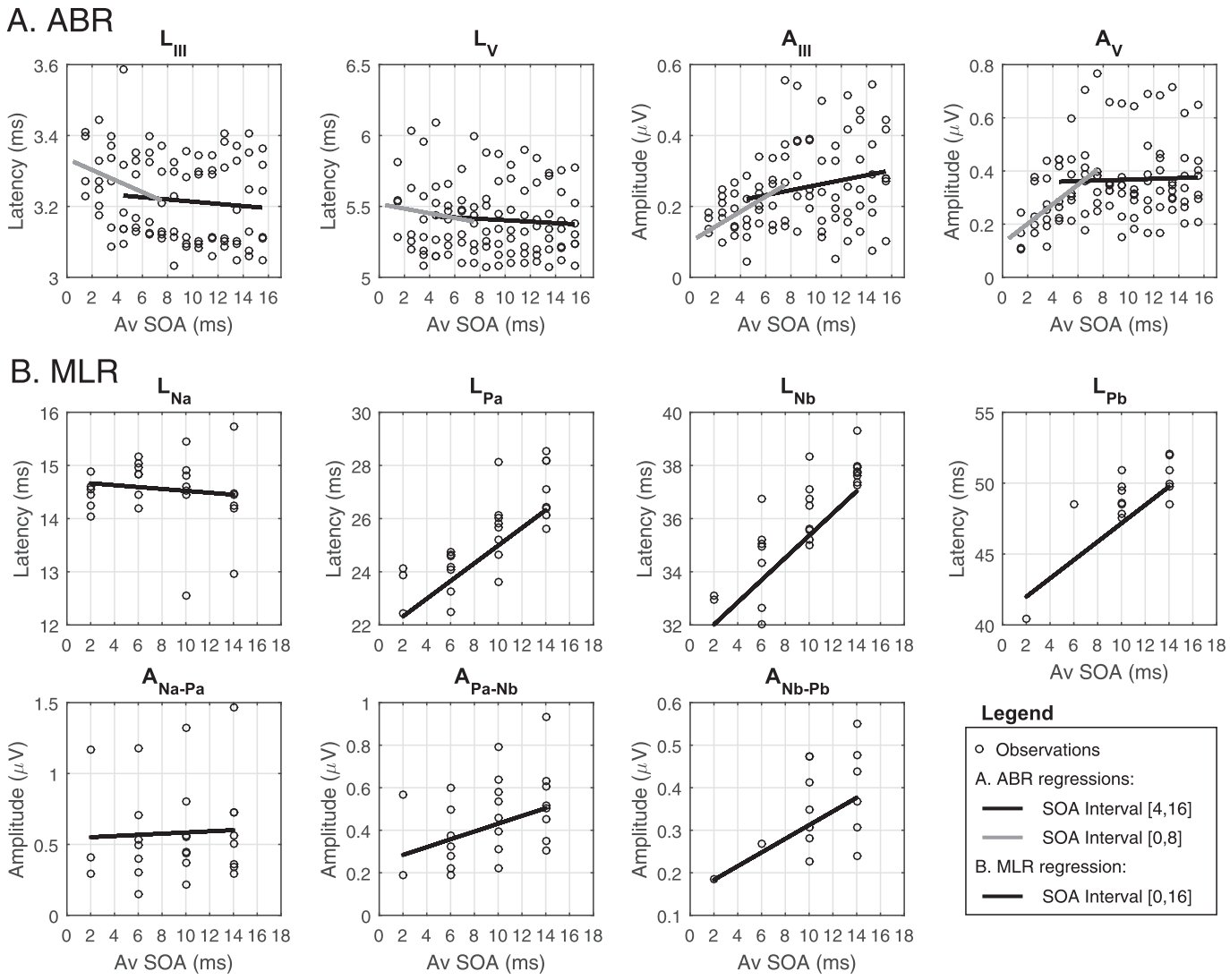

Fig. 5. Latencies (L) and amplitudes (A) of the main components of ABR (panel A) and MLR (panel B) signals obtained at the average SOA (Av SOA) of different rate-subsets. In panel A, the black and grey lines represent a linear regression analysis between the SOA intervals [4–16] and [0–8] ms, respectively. In panel B, the black line shows the linear regression analysis for the [0–16] ms SOA interval. The statistical analysis of these hypothesis tests are shown in Table 1.

Table 1
Statistic parameters of the linear regression hypothesis tests presented on Fig. 5.

	SOA interval	N	r	R2	p-value	a	SE(a)	b	SE(b)
Panel A									
L_{III}	[4–16]	71	−0.088	0.008	0.46	−0.003	0.004	3.244	0.047
L_{V}	[4–16]	84	−0.071	0.005	0.52	−0.005	0.008	5.452	0.087
A_{III}	[4–16]	71	0.196	0.039	0.10	0.007	0.004	0.190	0.048
A_{V}	[4–16]	84	0.036	0.001	0.74	0.001	0.005	0.353	0.050
L_{III}	[0–8]	40	−0.257	0.066	0.10	−0.016	0.010	3.334	0.054
L_{V}	[0–8]	44	−0.120	0.014	0.44	−0.016	0.022	5.517	0.122
A_{III}	[0–8]	40	0.448	0.200	0.0038*	0.021	0.007	0.101	0.039
A_{V}	[0–8]	44	0.495	0.245	0.00063*	0.037	0.010	0.128	0.058
Panel B									
L_{Na}	[0–16]	26	−0.121	0.015	0.56	−0.071	0.126	14.700	0.343
L_{Pa}	[0–16]	26	0.791	0.626	1.47e-06*	1.333	0.221	21.654	0.659
L_{Nb}	[0–16]	25	0.836	0.699	1.97e-07*	1.673	0.242	31.178	0.733
L_{Pb}	[0–16]	15	0.809	0.655	0.00026*	2.588	0.575	40.695	1.900
A_{NaPa}	[0–16]	26	0.049	0.002	0.81	0.017	0.073	0.543	0.216
A_{PaNb}	[0–16]	25	0.378	0.143	0.062#	0.073	0.040	0.247	0.120
A_{NbPb}	[0–16]	15	0.507	0.257	0.054#	0.064	0.033	0.151	0.111

N, number of observations; r, correlation coefficient; R^2, coefficient of determination; *p*-value, probability of rejecting the null hypothesis; a, angle slope; b, y-intercept; SE, standard error. * represents *p*-value < 0.05; # represents *p*-value ≈ 0.05.

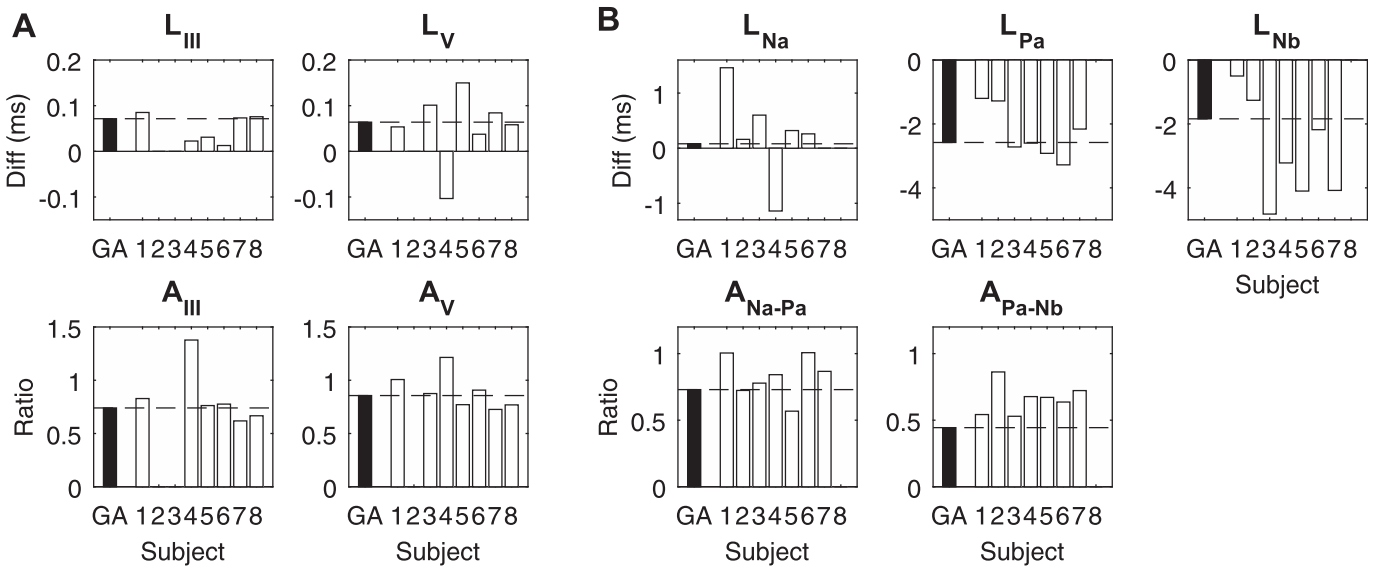

Fig. 6. Inter-subject variability of the fast adaptation. The fast adaptation was measured as the difference of latencies (in ms) and ratio of amplitudes between the averaged values corresponding to the intervals [1–8] ms and [8–16] ms, i.e. $L_{[1-8]}$-$L_{[8-16]}$ and $A_{[1-8]}/A_{[8-16]}$, both in ABR (panel A) and MLR (panel B) signals. Black boxes represent the estimates measured on the Grand-Average (GA) ABR/MLR waveforms, while the white boxes are the estimates for each individual subject.

2 in experiment 1 provide evidence that both fast and slow mechanisms of adaptation interact when presenting jittered stimuli. These fast and slow mechanisms of adaptation have been observed in a number of animal studies (Chimento and Schreiner, 1991; Eggermont, 1985; Javel, 1996; Yates et al., 1985; Westerman and Smith, 1984) and in ABR signals recorded with long- and short-SOA distributions (Valderrama et al., 2014b). If ABR/MLR waveforms in scenarios 1 and 2 were similar, it would be suggested that fast mechanisms of adaptation prevail over slow mechanisms, since the morphology of the response would be mostly influenced by the SOA of the preceding stimulus. In contrast, if ABR and MLR waveforms in scenario 2 were similar among themselves (and different to those obtained in scenario 1), that would indicate that slow mechanisms of adaptation prevail over fast mechanisms, since the morphology of the ABR/MLR signal would be determined by an averaged stimulation rate corresponding to several preceding stimuli. The results obtained in experiment 1 show that, in ABR signals on scenario 2, the latency of wave V remained constant across most of the sub-rates and that the amplitude decreased at a lower rate than in scenario 1. These results highlight the significant role of slow mechanisms of adaptation. The morphology of MLR signals in scenario 2 present significant variations among themselves, as a consequence of the fast mechanisms of adaptation, however in comparison with the MLRs on scenario 1, latencies seem less dependent on rate, amplitudes are smaller, and decrease with rate more slowly. These results point out the effects of both fast and slow mechanisms of adaptation.

The results obtained in experiment 3 are consistent with those obtained in experiment 1. These results show that the MLR waveforms obtained at different rate-subsets present significant variations as a consequence of the aforementioned fast and slow mechanisms of adaptation. This variability indicates that the time-invariant assumption is not accomplished all along the stimulation sequence. A direct consequence of this deviation from the time-invariant behavior is a degradation of the quality of the recordings, since the components are not phase-locked when the sweeps are averaged. The variability of the latencies observed in this study suggests that a possible strategy to improve the quality of the recordings could be the adjustment of the time-axis in each individual sweep in order to average phase-locked auditory responses.

In contrast to MLR, this study did not show differences in the morphology of ABR signals obtained at rate-subsets down to SOA_{4-5} (equivalent rate of 222 Hz), which shows the influence of the slow mechanisms of adaptation and that the time-invariant assumption is accomplished in this SOA range ([4–16] ms). The amplitudes of the ABR signals obtained at faster sub-rates present a significant decrease, indicating the prevalence of fast mechanisms of adaptation. The influence of the fast adaptation is particularly relevant at very fast rates, as in the SOA_{1-2} sub-sequence the ABR components could be detected in only a few subjects, and no subject showed any clear component at the SOA_{0-1} sub-sequence. The strong influence of the fast mechanisms of adaptation at these very fast rates could be associated with the refractory period of the neurons of the auditory pathway (Alvarez et al., 2011).

The results obtained in this study contradict the classical approach that claims that wide-jittered stimulation sequences can be a problem when assuming time-invariance of the response, since large SOA variations would evoke responses of different morphology. This classical approach only considers the fast mechanisms of adaptation. In contrast, this study highlights that both fast and slow mechanisms of adaptation influence the morphology of the evoked responses in jittered sequences, and therefore, both mechanisms should be considered when evaluating the time-invariant assumption in jittered stimulation sequences.

The mechanisms of adaptation have been attributed different functionalities in the auditory system. For example, the adaptive processes at different levels of the auditory pathway have been proven to enhance novelty detection (Ulanovsky et al., 2003), and to improve the neural coding accuracy by accommodating the rate-level function of the neurons to the characteristics of the input sound (Dean et al., 2005; Wen et al., 2009). The evaluation of the time-constants of the fast and slow mechanisms of adaptation observed in this study could have a potential clinical application in the future.

Future research could also investigate the manner in which the SOA jitter distribution influences the fast and slow adaptation mechanisms. The understanding of this relationship could help

design stimulation sequences with prevalence of the slow mechanisms of adaptation, thus accomplishing the time-invariance assumption.

5. Conclusions

This paper describes in detail the Split-iterative randomized stimulation and averaging (Split-IRSA) technique. This technique allows overlapping AEPs of different morphology to be disentangled through an iterative procedure in the time-domain. The results obtained with real and synthesized data indicate that the performance of this technique is robust when the parameter that controls convergence (α-value) and the number of iterations are adequately selected. A new strategy was designed to evaluate the time-invariant assumption on the AEP morphology in jittered sequences. The results point out that both fast and slow mechanisms of adaptation influence the AEP morphology, and therefore, both mechanisms should be taken into account when time-invariance is assumed.

Declaration of interest

The authors report no conflict of interest.

Acknowledgments

The authors of this paper acknowledge Dr. Harvey Dillon, Dr. Bram Van Dun and Dr. Fabrice Bardy (National Acoustic Laboratories, Sydney, Australia) for their comments and constructive input in previous drafts of this manuscript. This research is supported by the Australian Government through the Department of Health; by research project TEC2009-14245, Ministry of Finance and Competition (Government of Spain); and by Grant No. AP2009-3150, Ministry of Education, Culture and Sport (Government of Spain).

Appendix A. Supplementary data

Supplementary data related to this article can be found at http://dx.doi.org/10.1016/j.heares.2015.12.009.

References

Alvarez, I., de la Torre, A., Valderrama, J., Roldan, C., Sainz, M., Segura, J.C., Vargas, J.L., 2011. Changes over time of the refractory properties measured from ECAP in Pulsar CI^{100} cochlear implant recipients. J. Int. Adv. Otol. 7, 398–407.
Bardy, F., Dillon, H., Van Dun, B., 2014a. Least-squares deconvolution of evoked potentials and sequence optimization for multiple stimuli under low-jitter conditions. Clin. Neurophysiol. 125, 727–737.
Bardy, F., Van Dun, B., Dillon, H., McMahon, C.M., 2014b. Deconvolution of overlapping cortical auditory evoked potentials recorded using short stimulus onset-asynchrony ranges. Clin. Neurophysiol. 125, 814–826.
Bohórquez, J., Özdamar, Ö., 2008. Generation of the 40-Hz auditory steady-state response (ASSR) explained using convolution. Clin. Neurophysiol. 119, 2598–2607.
Burkard, R., Don, M., 2007. The auditory brainstem response. In: Burkard, R., Don, M., Eggermont, J. (Eds.), Auditory Evoked Potentials: Basic Principles and Clinical Application. Lippincott William & Wilkins, Baltimore, MD, pp. 229–253.
Burkard, R., Palmer, A.R., 1997. Responses of chopper units in the ventral cochlear nucleus of the anaesthetized guinea pig to clicks-in-noise and click trains. Hear. Res. 110, 234–250.
Burkard, R., Shi, Y., Hecox, K.E., 1990. A comparison of maximum length and legendre sequences for the derivation of brain-stem auditory-evoked responses at rapid rates of stimulation. J. Acoust. Soc. Am. 87, 1656–1664.
Chimento, T.C., Schreiner, C.E., 1991. Adaptation and recovery from adaptation in single fiber responses of the cat auditory nerve. J. Acoust. Soc. Am. 90, 263–273.
de Boer, J., Brennan, S., Lineton, B., Stevens, J., Thornton, A.R.D., 2007. Click-evoked otoacoustic emissions (CEOAEs) recorded from neonates under 13 hours old using conventional and maximum length sequence (MLS) stimulation. Hear. Res. 233, 86–96.
Dean, I., Harper, N., McAlpine, D., 2005. Neural population coding of sound level adapts to stimulus statistics. Nat. Neurosci. 8, 1684–1689.
Delgado, R.E., Özdamar, Ö., 2004. Deconvolution of evoked responses obtained at high stimulus rates. J. Acoust. Soc. Am. 115, 1242–1251.
Eggermont, J.J., 1985. Peripheral auditory adaptation and fatigue: a model oriented review. Hear. Res. 18, 57–71.
Eggermont, J.J., 1993. Wiener and Volterra analyses applied to the auditory system. Hear. Res. 66, 177–201.
Elberling, C., Kristensen, S.G.B., Don, M., 2012. Auditory brainstem responses to chirps delivered by different insert earphones. J. Acoust. Soc. Am. 131, 2091–2100.
Eysholdt, U., Schreiner, C., 1982. Maximum length sequences: a fast method for measuring brain-stem-evoked responses. Audiology 21, 242–250.
Hine, J.E., Thornton, A.R.D., Brookes, G.B., 1997. Effect of olivocochlear bundle section on evoked otoacoustic emissions recorded using maximum length sequences. Hear. Res. 108, 28–36.
Hine, J.E., Ho, C.-T., Slaven, A., Thornton, A.R.D., 2001. Comparison of transient evoked otoacoustic emissions thresholds recorded conventionally and using maximum length sequences. Hear. Res. 156, 104–114.
Javel, E., 1996. Long-term adaptation in cat auditory-nerve fiber responses. J. Acoust. Soc. Am. 99, 1040–1052.
Jewett, D.L., Caplovitz, G., Baird, B., Trumpis, M., Olson, M.P., Larson-Prior, L.J., 2004. The use of QSD (q-sequence deconvolution) to recover superposed, transient evoked-responses. Clin. Neurophysiol. 115, 2754–2775.
Jiang, Z.D., Brosi, D.M., Shao, X.M., Wilkinson, A.R., 2000. Maximum length sequence brainstem auditory evoked responses in term neonates who have perinatal hypoxiaischemia. Pediatr. Res. 48, 639–645.
Jiang, Z.D., Wu, Y.Y., Wilkinson, A.R., 2009. Age-related changes in BAER at different click rates from neonates to adults. Acta Paediatr. 98, 1284–1287.
Kjaer, M., 1980. Brain stem auditory and visual evoked potentials in multiple sclerosis. Acta Neurol. Scandivanica 62, 14–19.
Lasky, R.E., 1997. Rate and adaptation effects on the auditory evoked brain-stem response in human newborns and adults. Hear. Res. 111, 165–176.
Lasky, R.E., Maier, M.M., Liogier, X., Collet, L., 1995. Auditory evoked brainstem and middle latency responses in Macaca mulatta and humans. Hear. Res. 89, 212–225.
Leung, S., Slaven, A., Thornton, A.R.D., Brickley, G.J., 1998. The use of high stimulus rate auditory brainstem responses in the estimation of hearing threshold. Hear. Res. 123, 201–205.
Lineton, B., Thornton, A.R.D., Baker, V.J., 2006. An investigation into the relationship between input-output nonlinearities and rate-induced nonlinearities of click-evoked otoacoustic emissions recorded using maximum length sequences. Hear. Res. 219, 24–35.
Özdamar, Ö., Bohórquez, J., 2006. Signal-to-noise ratio and frequency analysis of continuous loop averaging deconvolution (CLAD) of overlapping evoked potentials. J. Acoust. Soc. Am. 119, 429–438.
Özdamar, Ö., Bohórquez, J., Ray, S.S., 2007. Pb(P1) resonance at 40 Hz: effects of high stimulus rate on auditory middle latency responses (MLRs) explored using deconvolution. Clin. Neurophysiol. 118, 1261–1273.
Stone, J.L., Calderon-Amulphi, M., Watson, K.S., Patel, K., Mander, N.S., Suss, N., Fino, J., Hughes, J.R., 2009. Brainstem auditory evoked potentials: a review and modified studies in healthy subjects. J. Clin. Neurophysiol. 26, 167–175.
Thornton, A.R.D., 2007. Instrumentation and recording parameters. In: Burkard, R., Don, M., Eggermont, J. (Eds.), Auditory Evoked Potentials: Basic Principles and Clinical Application. Lippincott William & Wilkins, Baltimore, MD, pp. 73–101.
Ulanovsky, N., Las, L., Nelken, I., 2003. Processing of low-probability sounds by cortical neurons. Nat. Neurosci. 6, 391–398.
Valderrama, J.T., Alvarez, I., de la Torre, A., Segura, J.C., Sainz, M., Vargas, J.L., 2012. Recording of auditory brainstem response at high stimulation rates using randomized stimulation and averaging. J. Acoust. Soc. Am. 132, 3856–3865.
Valderrama, J.T., de la Torre, A., Alvarez, I., Segura, J.C., Sainz, M., Vargas, J.L., 2014a. A flexible and inexpensive high-performance auditory evoked response recording system appropriate for research purposes. Biomed. Tech. 59, 447–459.
Valderrama, J.T., de la Torre, A., Alvarez, I., Segura, J.C., Thornton, A.R.D., Sainz, M., Vargas, J.L., 2014b. A study of adaptation mechanisms based on ABR recorded at high stimulation rate. Clin. Neurophysiol. 125, 805–813.
Valderrama, J.T., de la Torre, A., Alvarez, I.M., Segura, J.C., Thornton, A.R.D., Sainz, M., Vargas, J.L., 2014c. Auditory brainstem and middle latency responses recorded at fast rates with randomized stimulation. J. Acoust. Soc. Am. 136, 3233–3248.
Wen, B., Wang, G., Dean, I., Delgutte, B., 2009. Dynamic range adaptation to sound level statistics in the auditory nerve. J. Neurosci. 29, 13797–13808.
Westerman, L.A., Smith, R.L., 1984. Rapid and short-term adaptation in auditory nerve responses. Hear. Res. 15, 249–260.
Wong, P.K.H., Bickford, R.G., 1980. Brain stem auditory evoked potentials: the use of noise estimate. Electroencephalogr. Clin. Neurophysiol. 50, 25–34.
Yagi, T., Kaga, K., 1979. The effect of the click repetition rate on the latency of the auditory evoked brain stem response and its clinical use for a neurological diagnosis. Arch. Oto Rhino Laryngol. 222, 91–97.
Yates, G.K., Robertson, D., Johnstone, B.M., 1985. Very rapid adaptation in the guinea pig auditory nerve. Hear. Res. 17, 1–12.